Robustness of mode-locking in harmonic cavity nanolasers subjected to potential distortions

Yifan Sun, Sylvain Combrié, Alfredo de Rossi, Fabien Bretenaker

Research Article | Vol. 29, No. 4 / 15 February 2021 / Optics Express 5782

Optics EXPRESS

Robustness of mode-locking in harmonic cavity nanolasers subjected to potential distortions

YIFAN SUN,[1] SYLVAIN COMBRIÉ,[2] ALFREDO DE ROSSI,[2] AND FABIEN BRETENAKER[1,3,*]

[1] Université Paris-Saclay, CNRS, ENS Paris-Saclay, CentraleSupélec, LuMIn, 91405 Orsay, France
[2] Thales Research and Technology, 91120 Palaiseau, France
[3] Light and Matter Physics Group, Raman Research Institute, Bangalore 560080, India
[*] fabien.bretenaker@universite-paris-saclay.fr

Abstract: We theoretically analyze the robustness to potential distortion of mode-locking in a harmonic cavity nanolaser sustaining oscillation of Hermite-Gaussian modes. Different types of imperfections of the harmonic potential that create the Hermite-Gaussian modes are considered: the non-parabolicity of the potential and the possible random errors in the shape of the potential. The influence of the different laser parameters, including the Henry factors of the gain medium and the saturable absorber, on the robustness of the mode-locked regime is discussed in detail.

1. Introduction

Periodic optical pulses generated by mode-locked lasers are of particular importance for a wide range of applications, including high speed optical communications [1], biomedical imaging [2], remote sensing [3], timing synchronization [4], optical signal processing [5], materials processing [6], spectroscopy [7,8], etc. Among all possible sources, semiconductor mode-locked lasers are very attractive devices because they generate stable periodic pulses at very high repetition rates while being potentially very compact, cheap, efficient, and robust [9,10]. Nanolasers in particular have attracted intense interest because they are expected to be more compact, integrable, and energy efficient than conventional lasers [11].

Recently, a new type of photonic crystal cavity, sustaining oscillation of Hermite-Gaussian (HG) modes in a parabolic potential, has been proposed and demonstrated [12–14]. These cavities are attractive not only because of their compactness, but also because they exhibit a comb of equally spaced modes. Based on this remarkable property, we proposed a new type of passively mode-locked laser, obtainable by incorporating saturable gain and absorber sections in such a cavity. In such a laser, the pulse repetition rate depends on the curvature of the potential instead of the cavity length [15]. In addition, different dynamical laser behaviors, including self-starting regimes, were investigated, such as Q-switching, Q-switched mode locking, continuous-wave mode locking, etc. [16].

However, potential practical implementation of such a mode-locked laser needs to take into account different types of defects that may affect the resonator. This is particularly true due to the fact that realization of such lasers relies on nano-fabrication techniques. For example, there might be some disorder in the size and position of the lattice holes [17–23], or simply some surface roughness or variation of the thickness of some layers [17,18,24–27]. Such general fabrication-related defects [19] may influence properties such as the band structure [18,27–33], the attenuation [21,28,31,33–37], or the coupling strength between cavities [38]. Usually such a disorder is undesirable except to obtain random laser operation [39–41], to observe Anderson localization [18,31,42–44], or to induce new functionalities [45,46]. Some new methods to probe disorder induced distortion in photonic devices have been developed [47,48]. Also, it has recently been shown that the intensity variations due to the disordered medium can be entirely suppressed by adding disorder-specific gain and loss components to the medium [49,50].

#418342 https://doi.org/10.1364/OE.418342
Journal © 2021 Received 23 Dec 2020; revised 25 Jan 2021; accepted 28 Jan 2021; published 8 Feb 2021

Optics EXPRESS

In the lasers that we consider, we can take most of these effects into account by introducing some distortion in the harmonic potential. Such a modification of the potential should be expected to lead to a modification of the Hermite-Gaussian modes and to a distortion of the cavity mode spectrum with respect to a perfect frequency comb. The question then arises to know whether the mode locking regime of operation will be robust with respect to such alterations of the cavity mode spectrum, which are unavoidable whatever the fabrication process. Thanks to the nonlinear nature of mode locking, in general, semiconductor mode-locked lasers are very robust. Even the locking of multi-mode fiber lasers is robust to disorder [51–54]. But this question needs to be addressed in the peculiar case of harmonic cavity nanolasers.

The aim of this paper is thus to investigate the robustness of mode locking of the Hermite-Gaussian modes in an harmonic cavity nanolaser from a theoretical and simulation standpoint. We focus on two different kinds of distortion of the harmonic potential. The first one is the non-parabolicity of the potential, which could for example be simply due to errors in the positioning of the elements of the structure. A fourth-order term is introduced in the potential to quantify this deformation. This distortion can strongly alter the Hermite-Gaussian modes and shift the initially equally spaced frequencies. The second type of potential distortion we consider consists in random errors in the shape of the potential, somewhat simulating disorder due to different kinds of structural imperfections. To this aim, a Gaussian random function with zero mean value is added to the potential. In both cases, we compare the mode spectrum of the "cold" cavity with the laser spectrum, in order to isolate the capability of the laser nonlinearities to restore mode-locked operation. We also take into account the existence of a non-zero Henry factor for the gain medium and the absorber.

The paper is organized as follows: Section 2 introduces the model and the two kinds of potential distortion. Section 3.1 focuses on the investigation of the effect of the non-parabolicity of the potential. Section 3.2 describes the laser behavior in the presence of disorder created using random errors in the shape of the potential. The evolution of the laser behavior is then statistically investigated, including the influence of the Henry factor. Section 4 gives the conclusions of the paper.

2. Harmonic cavity laser with imperfect potential

The starting point is the master equation initially developed in Refs. [15,16] to describe the evolution of light in a nanolaser based on a harmonic potential for light and containing a gain medium and a saturable absorber. The time evolution of the slowly varying amplitude $A(x,t)$ of the field inside the unidimensional cavity can be described by:

$$i\frac{\partial A}{\partial t} + \left[\frac{1}{2}\omega_{kk}\frac{\partial^2 A}{\partial x^2} - \frac{1}{2}\frac{\Omega^2}{\omega_{kk}}x^2 A\right] - iH_1(|A|^2)A = 0\,, \tag{1}$$

where ω_{kk} is the second-order derivative of the dispersion at the bandgap edge of the photonic crystal and Ω is the free spectral range (FSR) of the harmonic resonator. This cavity effect is described by the two terms in square brackets, which are a combination of the dispersion property of the photonic bandgap structure and the parabolic potential created by slowly spatially varying one of the structure parameters.

The three first terms in Eq. (1) lead to the existence of Hermite-Gaussian eigenmodes. The red full line in Fig. 1(a) shows the parabolic potential created by the term proportional to x^2. It also shows the spectrum of equally separated eigenfrequencies (the free spectral range $\Omega/2\pi$ is chosen equal to 100 GHz), together with the shapes of their associated Hermite-Gaussian (HG) modes.

The dissipative term H_1 describes the effects of the gain medium, the losses, and the saturable absorption:

$$H_1 = \frac{1}{2}g(x,t)(1 - \mathrm{i}\alpha_\mathrm{g}) - \frac{1}{2}a(x,t)(1 - \mathrm{i}\alpha_\mathrm{a}) - \frac{1}{2}\gamma_0\,, \tag{2}$$

Optics EXPRESS

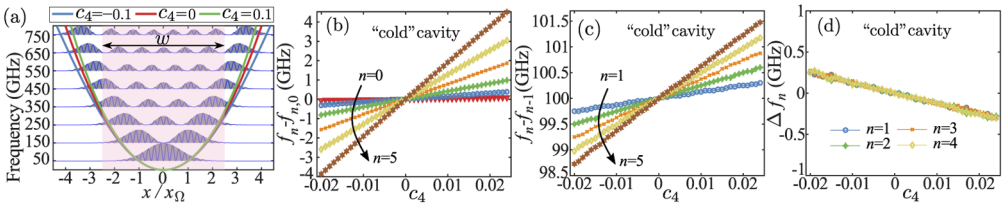

Fig. 1. (a) Hermite-Gaussian modes in a parabolic potential, with three different values of the non-parabolicity coefficient c_4. Semi-transparent pink area: active media. (b-d) Evolution of the mode characteristics of the "cold" cavity versus c_4. (b) Frequency deviations $f_n - f_{n,0}$; (c) frequency separations $f_n - f_{n-1}$ between successive modes; (d) frequency differences $\Delta f_n = 2f_n - f_{n+1} - f_{n-1}$.

where γ_0 holds for the intrinsic losses, g and a are the gain and absorption coefficients per unit time, and α_g and α_a are the associated Henry factors for gain and absorption, respectively.

The saturation of the gain and of the absorption is described by the following set of spatially local equations:

$$\frac{\partial g(x,t)}{\partial t} = -\frac{g(x,t) - g_0(x)}{\tau_g} - \frac{|A(x,t)|^2}{\tau_g I_{sat,g}} g(x,t)\,, \tag{3}$$

$$\frac{\partial a(x,t)}{\partial t} = -\frac{a(x,t) - a_0(x)}{\tau_a} - \frac{|A(x,t)|^2}{\tau_a I_{sat,a}} a(x,t)\,, \tag{4}$$

where $g_0(x)$ and $a_0(x)$ are the unsaturated gain and absorption coefficients. In the present paper, for the sake of simplicity, we suppose that $g_0(x)$ and $a_0(x)$ are homogeneously distributed in the same region of the cavity centered around its center (pink shaded area in Fig. 1(a)). The durations τ_g and τ_a represent the lifetimes of the gain and the absorption and $I_{sat,g}$ and $I_{sat,a}$ are the corresponding saturation intensities . The field $A(x,t)$ inside the cavity can be expanded on the basis of the Hermite-Gaussian modes $\Psi_n(x)$ shown in Fig. 1(a):

$$A(x,t) = \sum_{n=0}^{\infty} C_n(t) e^{-i\omega_n t} \Psi_n(x)\,, \tag{5}$$

with the eigenfrencies

$$\omega_n = \left(n + \frac{1}{2}\right)\Omega\,. \tag{6}$$

For a given field distribution $A(x,t)$, the slowly varying modal coefficient $C_n(t)$ can be calculated by projecting the field amplitude on Ψ_n:

$$C_n(t) = e^{i\omega_n t} \int_{-\infty}^{\infty} A(x,t)\Psi_n(x)dx. \tag{7}$$

2.1. Non-parabolicity of the potential

If the potential is not a perfect parabola, the HG modes in the cavity get distorted. The frequency difference between successive modes is then no longer uniform, and the cavity spectrum does no longer form a perfect frequency comb. For example, the mode frequencies should decrease (increase) if the potential is wider (narrower) than a perfect parabola.

To investigate the influence of such an anharmonicity on the mode locking, we introduce extra terms to the term proportional to x^2 in Eq. (1). Since an asymmetry of the cavity would play only a minor role, as shown in Supplement 1, we ignore here third-order terms. We thus add a fourth-order term to the parabolic potential in order to quantify the distortion. Since the size of

Optics EXPRESS

the cavity is determined from the scaling factor $x_\Omega = \sqrt{\omega_{kk}/\Omega}$, the master equation (Eq. (1)) in the presence of distortion can be written in the following normalized form:

$$\begin{aligned} \mathrm{i}\frac{1}{\Omega}\frac{\partial A}{\partial t} = &\left[-\frac{1}{2}x_\Omega^2\frac{\partial^2 A}{\partial x^2} + \frac{1}{2}\left(\frac{x}{x_\Omega}\right)^2 + \frac{c_4}{4!}\left(\frac{x}{x_\Omega}\right)^4\right]A \\ &+ \frac{\gamma_0}{2\Omega}\left[\frac{g(1-\mathrm{i}\alpha_\mathrm{a})}{\gamma_0} - \frac{a(1-\mathrm{i}\alpha_\mathrm{a})}{\gamma_0} - 1\right]A\,, \end{aligned} \tag{8}$$

where c_4 is a dimensionless coefficient characterizing the amplitude of the distortion.

2.2. Potential disorder

We can follow a similar method to introduce the effect of random errors in the shape of the potential. To this aim, a term $D_\mathrm{max}R(x)$ is added to the potential, where $R(x)$ is a standard centered Gaussian random variable with variance 1. The amplitude of the disorder is adjusted by varying D_max. The master equation can then be written as

$$\begin{aligned} \mathrm{i}\frac{1}{\Omega}\frac{\partial A}{\partial t} = &-\frac{1}{2}x_\Omega^2\frac{\partial^2 A}{\partial x^2} + \left[\frac{1}{2}\left(\frac{x}{x_\Omega}\right)^2 + D_\mathrm{max}R(x)\right]A \\ &+ \frac{\gamma_0}{2\Omega}\left[\frac{g(1-\mathrm{i}\alpha_\mathrm{g})}{\gamma_0} - \frac{a(1-\mathrm{i}\alpha_\mathrm{a})}{\gamma_0} - 1\right]A\,. \end{aligned} \tag{9}$$

3. Results and discussion

In this section we numerically simulate Eqs. (8) and (9) to predict the laser behavior in the presence of potential distortion. To this aim, like in Ref. [16], we use the split-step Fourier method. The spatial discretization period is equal to 0.13 x_Ω. The time discretization period is equal to 10 fs for all simulations. We have checked that it is small enough to ensure a good accuracy for all the cases studied in this paper. As the gain width is fixed at $w = 5x_\Omega$, the intensities of only the first six modes are significantly different from zero. Therefore, in the following, only modes labeled $n = 0 \cdots 5$ are taken into account.

In this section, we check whether the laser modes are locked using three different ways. The first one is to monitor the relative phase differences $\Delta\phi_n = 2\phi_n - \phi_{n+1} - \phi_{n-1}$, which are obtained from the arguments of the $C_n(t)$'s in Eq. (7). The second one consists in calculating the frequency separations between the modes in the presence of distortion, in order to check whether the laser operation restores equally spaced frequencies. The last one consists of course in looking at the regularity of the generated pulse train.

3.1. Non-parabolicity of the potential

Three examples of distorted potentials with different values of c_4 are shown in Fig. 1(a). A positive value of c_4 leads to a narrower potential, and vice versa. The gain and absorber are supposed to spatially overlap in the middle of the cavity (transparent pink region of Fig. 1(a)).

Before studying the laser behavior in the presence of anharmonicity, we first calculate the eigenfrequencies of the "cold" cavity in the presence of distortion. To this aim, a random noise field is injected inside the cavity as initial value for the field. Then we compute the evolution of this field according to Eq. (9) with $\gamma_0 = 0$, $a_0 = 0$, and $g_0 = 0$, i. e. in the absence of any losses or gain. In these conditions, the "cold" cavity works as a spectral filter. The calculation is run during 30 ns. Then the spectrum $F(2\pi f)$ of the intracavity field is calculated using the following

Optics EXPRESS

expression:

$$F(2\pi f) = \int_{-\infty}^{+\infty} \left| \int_{-\infty}^{+\infty} A(x,t) e^{i2\pi ft} dt \right|^2 dx. \quad (10)$$

This equation is applied to the evolution of the field $A(x,t)$ during the last 24 ns of the simulation. The eigenfrequencies f_n of the cold cavity are then obtained by finding the peaks in the spectrum $F(2\pi f)$.

Figure 1(b) shows the result of such simulations for varying values of c_4. Each line corresponds to the evolution of $f_n - f_{n,0}$, for $n = 0, \ldots, 5$, where $f_{n,0} = \omega_n/2\pi = (n + 1/2)\Omega/2\pi$ is the eigenfrequency for $c_4 = 0$. One can see that these frequency shifts $f_n - f_{n,0}$ linearly increase as c_4 increases, and that the slope increases with the mode order n. By looking at the frequency difference $f_n - f_{n-1}$ between successive modes, as shown in Fig. 1(c), one notices that the potential distortion $c_4 \neq 0$ destroys the periodicity of the frequency comb. The mode separation is larger than the initial value of 100 GHz for c_4>0, and conversely. Moreover, for a given value of c_4, one can see that the frequency separation between successive modes increases linearly with n. This can be seen from Fig. 1(d), showing that $\Delta f_n = 2f_n - f_{n+1} - f_{n-1} = (f_n - f_{n-1}) - (f_{n+1} - f_n)$ is independent of n.

The question then arises to know whether the nonlinearity of the active medium and of the saturable absorber is still sufficient to obtain mode locked operation, i. e. to restore the periodicity of the comb of modes, even for $c_4 \neq 0$. We suppose here for example that the gain and absorber regions have a width $w = 5x_\Omega$ and spatially overlap in the cavity center, as represented by the transparent pink region in Fig. 1(a). The values of the parameters are chosen as follows: intrinsic losses lead to a dissipation rate $\gamma_0 = 10^{10}$ s^{-1}, the relative unsaturated gain coefficient is $r_g = g_0/\gamma_0 = 70$, and the relative unsaturated absorption coefficient is $r_a = a_0/\gamma_0 = 10$. The value of the gain lifetime is $\tau_g = 1$ ns, and the absorber lifetime is $\tau_a = 10$ ps. The ratio between the saturation energies of the gain and absorber media is $R_E = E_{sat,g}/E_{sat,a} = 25$. In the following, three examples are investigated in details.

These three examples of the time evolution of the laser, corresponding to $c_4 = -0.01$, $c_4 = 0.01$, and $c_4 = 0.02$, are plotted in Fig. 2. Let us first look at Fig. 2(a), which has been obtained for $c_4 = -0.01$. The upper plots show the time evolution of the mode intensities $|C_n|^2$ and of the relative phase differences $\Delta\phi_n = 2\phi_n - \phi_{n+1} - \phi_{n-1}$ between the modes. We can see that all the mode intensities are modulated. Furthermore, the phase difference $\Delta\phi_1$ varies in a monotonous manner versus time, corresponding to a beat frequency of the order of 300 MHz, while all other phase differences $\Delta\phi_n$ for $n = 2, 3, 4$ are locked. This means that all the modes are phase locked except mode $n = 0$. This unlocked mode is responsible for the modulation of the intensity $|A_+(x = 0, t)|^2$ of the field propagating in the $+x$ direction at cavity center $x = 0$, which is shown in the two plots of Fig. 2(b). This indicates that mode 0 is more easily influenced by the distortion of the potential when c_4<0 and then loses the locking.

On the contrary, with $c_4 = 0.01$ and all other parameters left unchanged, Figs. 2(c) and (d) shows that all the modes are locked. All modulations have disappeared in the mode intensities and relative phases, and the peak intensity of $|A_+(x = 0, t)|^2$ remains stable with time, equal to 80 $I_{sat,g}$, as can be seen in Fig. 2(d).

However, if c_4 is further increased up to $c_4 = 0.02$, Figs. 2(e) and (f) show that some modes get unlocked, leading again to a modulation of the peak values of $|A_+(x = 0, t)|^2$.

From the above results, it is clear that there exists a locking region between $c_4 = -0.01$ and $c_4 = 0.02$, for which all modes can be locked. The same calculation is thus performed for varying values of c_4. The frequencies f_n of the modes are obtained by calculating the spectrum of the field within the last 24 ns of the simulation once the laser is in steady-state regime. The results are plotted in Fig. 3. Figure 3(a) shows the peak intensities observed at the center of the cavity for light traveling in the $+x$ direction, while Figs. 3(b)-(d) are presented in a similar manner as the results for the cold cavity shown in Figs. 1(b)-(d).

Optics EXPRESS

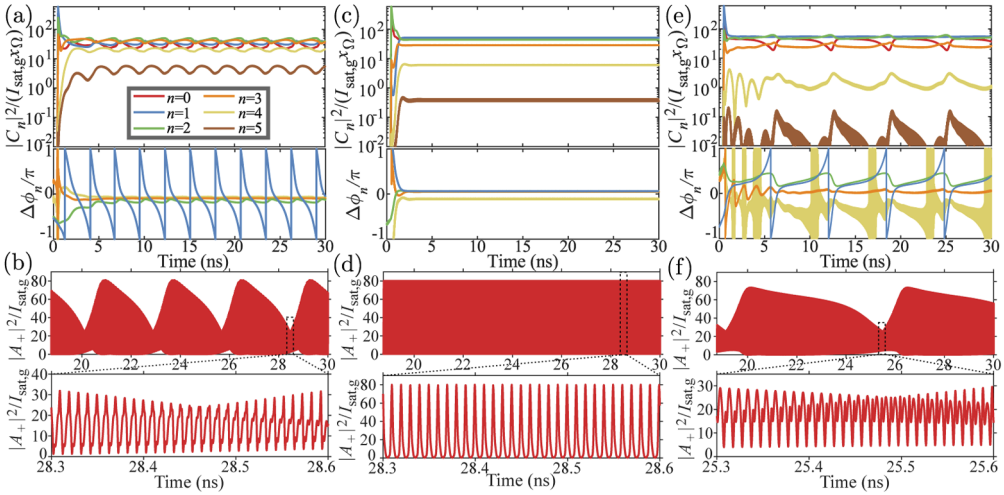

Fig. 2. Steady-state time evolution of (a,c,e) the laser mode intensities and phase differences and (b,d,f) the laser intensity traveling in the $+x$ direction at cavity center ($x = 0$) for (a,b) $c_4 = -0.01$ (partial mode-locking), (c,d) $c_4 = 0.01$ (perfect mode-locking), (e,f) $c_4 = 0.02$ (partial mode-locking). Other parameter values: $r_g = g_0/\gamma_0 = 70$, $r_a = a_0/\gamma_0 = 10$, $w = 5x_\Omega$, $\tau_g = 1$ ns, $\tau_a = 10$ ps, $\gamma_0 = 10^{10}$ s^{-1}, $\Omega/2\pi = 100$ GHz, $E_{sat,g}/E_{sat,a} = 25$, $\alpha_g = \alpha_a = 0$.

Figure 3(b) shows that the mode frequencies f_n increase as c_4 increases. The shift of higher order modes is larger than that for lower order modes. But the comparison with Fig. 1(b) shows that the mode frequency shifts $f_n - f_{n,0}$ are clearly reduced by the nonlinearity of the active media, especially for $c_4 > 0$. It is clear that f_0 does no longer follow the same evolution when $c_4 < -0.007$.

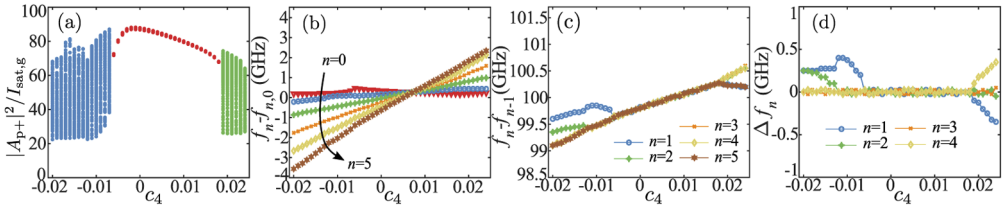

Fig. 3. Evolution of the steady-state laser characteristics versus c_4. (a) Peak intensities of the field propagating in the $+x$ direction at $x = 0$. (b) Frequency deviations $f_n - f_{n,0}$; (c) frequency separations $f_n - f_{n-1}$ between successive modes; (d) frequency differences $\Delta f_n = 2f_n - f_{n+1} - f_{n-1}$. Same parameter values as in Fig. 2.

Figure 3(c) shows that there exists an asymmetric locking region for $-0.007 \le c_4 \le 0.019$. With comparison with Fig. 2, one can see that the laser nonlinearity tends to reduce the frequency separation between the modes. It is thus more efficient to induce mode locking for positive values of c_4 than for negative values. In the locking region, for a given value of c_4, the mode separation is the same for all values of n and linearly increases with c_4. In addition, one can notice that the mode frequency separation for $c_4 = 0$ is reduced to 99.8 GHz due to the nonlinearity of active media. Outside this locking region, some modes are still locked, as can be seen from Fig. 3(d). Some of the modes still obey $\Delta f_n = 0$, indicating that the corresponding mode frequencies are equally spaced. This is a big difference with respect to Fig. 1(d), induced by the nonlinearity of the amplifying and absorbing media.

Optics EXPRESS

Based on Figs. 2 and 3, we can see that there are several ways to observe the locking. The first one is to look at the phase difference $\Delta\phi_n$ between the modes, as can be seen by comparing Figs. 2(a) and 2(c). The second method consists in observing the frequency difference between successive modes, such as $f_n - f_{n-1}$ in Fig. 3(c) or $\Delta\phi_n$ in Fig. 3(d). These criteria are corroborated by observing the evolution of the peak intensities like in the three examples of Figs. 2(b),(d), and (f) and also summarized in Fig. 3(a). This plot shows all the peak intensities $|A_{p+}|^2$ of the field propagating into the $+x$ direction at $x = 0$ detected during the last 10 ns of each simulation. If all the modes are locked, this peak intensity has only one value as shown by the red dots in Fig. 3(a).

Outside the locking region, some modes are unlocked, leading to a slow modulation of the intensity, as is visible in the cases of Figs. 2(b) and (f). It also leads to several peak intensity values, as shown by the blue and green dots of Fig. 3(a). Unlocking is confirmed by the evolutions of the frequencies f_n in Figs. 3(c) and (d).

Figure 4(a) shows the evolution of the locking range with the unsaturated gain and absorption rates $r_g = g_0/\gamma_0$ and $r_a = a_0/\gamma_0$. The two surfaces in this figure correspond to the two extremes values of c_4 between which all the laser modes are locked. In all cases, the upper limit for c_4 is larger than the lower limit, as already observed in Fig. 3(a). The locking range increases almost linearly with the saturable absorption rate r_a, except on the positive c_4 side where it decreases for large values of r_a. This corresponds to situations where the laser is close to the border to Q-switching regime [16].

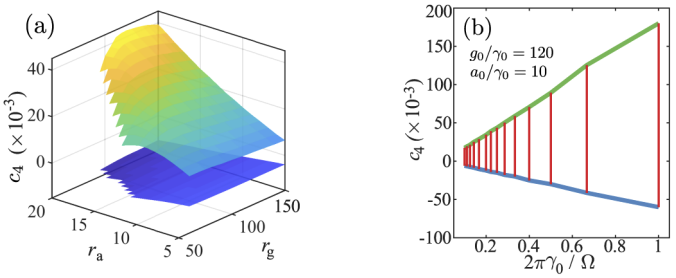

Fig. 4. (a) Evolution of the mode-locking threshold values for c_4 versus r_a and r_g. (b) Evolution of the locking region (red region) versus γ_0. $g_0/\gamma_0 = 120$ and $a_0/\gamma_0 = 10$ are fixed. Same parameter values as in Fig. 2.

If the ratios $r_g = g_0/\gamma_0 = 120$ and $r_a = a_0/\gamma_0 = 10$ are fixed, varying the intrinsic losses γ_0 leads to the evolution of the locking region plotted in Fig. 4(b). The width of the region linearly increases with γ_0. In fact, this increase is due to the increase in saturable absorption a_0. At the same time, the increase in gain g_0 ensures that the laser is far away from the Q-switching region.

3.2. *Potential disorder*

The non-parabolicity of the potential can be regarded as a special kind of distortion. Here we extend the investigation of the robustness of mode locking from the influence of non-parabolicity to the influence of random errors in the shape of the potential. A term $D_{max}R(x)$ is thus added to the potential to describe this disorder, as given by Eq. (9). When the laser reaches its steady-state regime, the method of Eq. (10) is implemented to calculate the mode frequencies f_n.

To assess whether the laser remains locked in the presence of disorder, we define the free spectral range (FSR) relative root mean square (RMS) deviation δ:

$$\delta = \frac{1}{\Delta f}\sqrt{\frac{1}{N}\sum_{n=0}^{N-1}|f_n - f_{fit}(n)|^2}, \tag{11}$$

Optics EXPRESS

where $f_{\mathrm{fit}}(n)$ is a linear fit of the evolution of the f_n's with n and $\Delta f = f_{\mathrm{fit}}(n) - f_{\mathrm{fit}}(n-1)$ is the mode separation obtained from the fit.

Before applying this criterion to the case of the disordered potential, let us first test its usefulness by applying it to the case of the non-parabolicity of the potential studied in the preceding subsection. We thus calculate δ according to Eq. (11) for the data of Figs. 1(b)-(d) and 3. We start with the "cold" cavity data of Fig. 1(b)-(d) and plot the corresponding FSR relative RMS deviations δ_C versus c_4 as open circles in Fig. 5(a). We then retrieve the linear evolution of the cold cavity FSR versus c_4, which was already observed in Figs. 1(c) and (d). The same treatment is applied to the laser data of Figs. 3(b)-(d), leading to the evolution of δ_L versus c_4 shown as triangles in Fig. 5(a). The locking region, in which δ_L remains equal to zero, is clearly visible in this figure. This shows that δ can be used as a criterion to recognize mode locked operation.

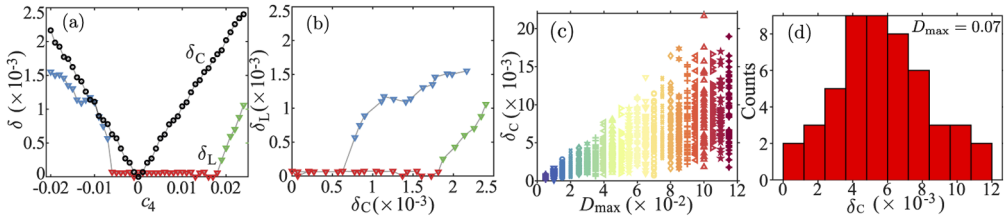

Fig. 5. (a) FSR relative RMS deviations δ_L and δ_c as a function of c_4. (b) Map of δ_L versus δ_C for the same values of c_4 as in (a). The blue (green) triangles correspond to unlocked solution with c_4<0 (c_4>0). The data for (a) and (b) are from Fig. 3 and Figs. 1(b)-(d). (c) Distribution of cold cavity FSR relative RMS deviation δ_C versus D_{max}. The calculation is run 50 times for each value of D_{max}. (d) Example of histogram of δ_C for D_{max} = 0.07.

It is worth observing the evolution of δ_L versus δ_C, when c_4 is varied, as plotted in Fig. 5(b). It is clear that there exists a threshold value for δ_C below which locking is preserved.

The same method is implemented to calculate the FSR relative RMS deviation δ_C for the "cold" cavity for a randomly disordered potential. We run the simulation for 30 ns, removing the active media and losses ($\gamma_0 = 0$, $a_0 = 0$, $g_0 = 0$). The spectra are obtained from the last 24 ns of each simulation, so that the frequency resolution is 0.042 GHz. The eigenfrequencies are extracted from the peaks of the field spectrum following Eq. (10) and used to calculate δ_C according to Eq. (11). This leads to the evolution of δ_C versus D_{max}, which is plotted in Fig. 5(c). Because of the random character of the potential disorder, the calculation is run 50 times for each value of D_{max}. Hence, in total this figure contains 1150 different solutions for 23 different values of D_{max}. The general trend is that the range of values of δ_C increases linearly with D_{max}. One example of histogram of δ_C for D_{max} = 0.07 is shown in Fig. 5(d).

To evaluate the robustness of mode locking to disorder, the RMS deviation δ_L is calculated for laser operation with the same parameters as in the preceding subsection and including the same potential disorder as in the case of the cold cavity. The results for r_a = 10 and r_g = 150 are shown in Figs. 6(a)-(d). Obtained from 1150 solutions for 23 different values of D_{max}, the values of δ_L are plotted as a function of D_{max} in Fig. 6(a). Some values of δ_L drop to 0, contrary to what was happening in Fig. 5(c). Especially, for D_{max} = 0.005, all the values of δ_L are close to 0. This indicates that an equally spaced comb is formed by mode locking.

Since we used exactly the same disordered potential in both cases, we can plot the value of δ_L versus δ_C , as shown in Fig. 6(b). We notice that there exists a threshold value $\delta_{C,th}$ of δ_C below which the laser remains locked. This means that the nonlinear locking effect can somewhat compensate the disorder in the potential.

To define and find this threshold value $\delta_{C,th}$, we first plot the histogram of δ_L for all the solutions (see Fig. 6(c)). It is clear that the histogram of δ_L can be divided into two different

Optics EXPRESS

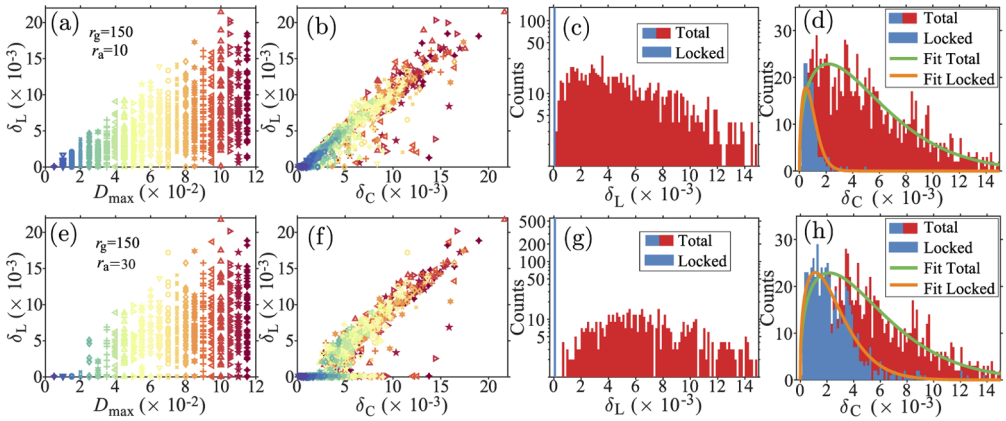

Fig. 6. (a,e) Distribution of laser FSR relative RMS deviation δ_L versus D_{max}. (b,f) Evolution of δ_L versus δ_C. (c,g) Corresponding histograms of δ_L for all solutions (red) and solutions exhibiting mode locking (blue). (d,h) Same as (b,f) versus δ_C. The fits are obtained from a Weibull distribution. (a-d) $r_a = 10$, $r_g = 150$; (e-h) $r_a = 30$, $r_g = 150$. All other parameter values are the same as in Fig. 2.

regions. The unlocked solutions distribute along a wide range of values of δ_L (marked by red bars). However, there are 153 solutions located in the first bin within the range $[0, 1.51 \times 10^{-4}]$ of values of δ_L (marked by blue bars). Figure 6(d) compares a histogram of the values of δ_C corresponding to mode locked operation, together with a histogram of all the values of δ_C. One can notice that only a portion of the solutions with rather small values of δ_C are locked. From this figure, we can define $\delta_{C,th}$ as the threshold value above which less than 50% of simulations lead to mode locking.

One way to directly find $\delta_{C,th}$ would be to simply calculate the ratio between the number of locked solutions and the total number of simulations for each value of δ_C. However, this strongly depends on the number and width of the bins in the histogram. To circumvent this problem, we fit the histograms using a Weibull distribution. The probability density function (PDF) of a Weibull random variable is expressed as

$$f(x;\lambda,k) = \begin{cases} \frac{k}{\lambda}\left(\frac{x}{\lambda}\right)^{k-1} e^{-(x/\lambda)^k} & x \geq 0\,, \\ 0 & x<0\,, \end{cases}$$

where $k>0$ is the shape parameter and $\lambda>0$ is the scaling parameter of the distribution.

The results of these fits are shown as full lines in Fig. 6(d), where the fit parameters are $\lambda = 5.61$ and $k = 1.37$ for the ensemble of all solutions and $\lambda = 0.98$ and $k = 1.53$ for mode-locked solutions. This leads to the threshold value $\delta_{C,th} = 1.2 \times 10^{-3}$, evaluated as the value of δ_C for which the ratio of the two distributions is 0.5.

The same calculations are performed for $r_a = 30$, $r_g = 150$. The corresponding results are plotted in Figs. 6(e)-(h). The fit parameters are unchanged for the ensemble of solutions and become $\lambda = 2.7521$ and $k = 1.395$ for the mode-locked solutions. We obtain in this case a larger threshold value $\delta_{C,th} = 3.8 \times 10^{-3}$ for mode-locking.

Using this method, we calculate the evolution of $\delta_{C,th}$ as a function of r_a, which is shown in Fig. 7(a) for different values of r_g. The threshold $\delta_{C,th}$ increases linearly with the saturable absorption rate r_a. However, the solutions finally approach the limit of Q-switching when r_a is increased. This leads to a sharp decrease in $\delta_{C,th}$. On the contrary, increasing r_g can keep away from that border so that higher values of r_a can be allowed. This indicates that the robustness of locking to the disorder increases with the saturable absorption rate r_a.

Optics EXPRESS

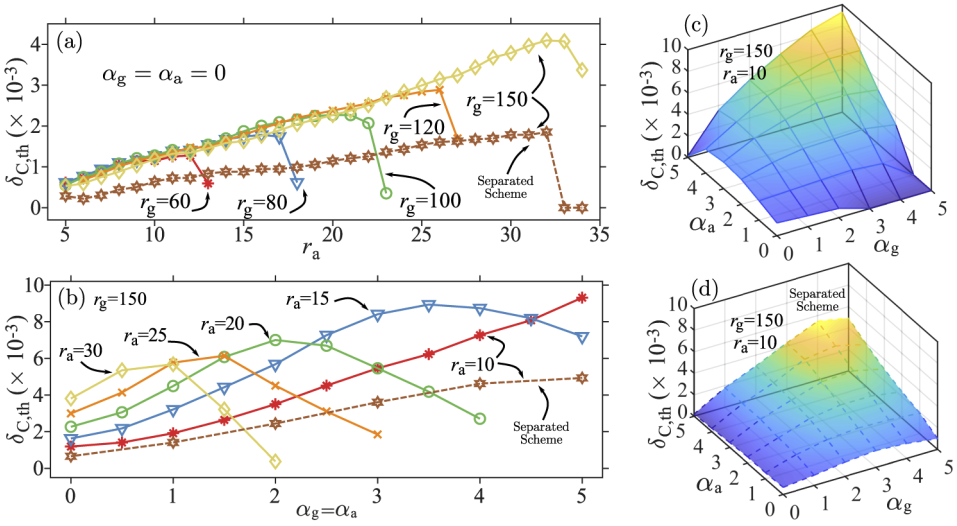

Fig. 7. Evolution of the mode-locking threshold value of $\delta_{C,th}$ with different parameters: (a) δ_C versus r_a for $\alpha_g = \alpha_a = 0$ and several values of r_g; (b) δ_C versus $\alpha_g = \alpha_a$ for several values of r_a and $r_g = 150$; (c-d) δ_C versus α_g and α_a for $r_a = 10$ and $r_g = 150$. The dashed lines in each subfigure represent the solutions for the case where the gain region is located in the region $-2.5\ x_\Omega \le x \le 0$ and the absorber in the region $0 \le x \le 2.5\ x_\Omega$. Other parameter values: $w = 5x_\Omega$, $\tau_g = 1$ ns, $\tau_a = 10$ ps, $2\pi\gamma_0/\Omega = 0.1$ and $E_{sat,g}/E_{sat,a} = 25$.

The same technique is used to investigate the influence of the Henry factors α_g and α_a of the gain medium and the absorber, respectively. For simplicity, we take $\alpha_g = \alpha_a$ and plot in Fig. 7(b) the evolution of $\delta_{C,th}$ as a function of $\alpha_g = \alpha_a$, with $r_g = 150$ and for different values of r_a.

It is interesting to notice that the Henry factor first increases the threshold $\delta_{C,th}$. In other words, it increases the robustness of mode-locking to disorder, especially for small values of r_a. But, clearly, a large value of the Henry factors is detrimental to locking, as reported in several Refs. [16,55,56], so that the threshold $\delta_{C,th}$ eventually decreases.

We also investigate the robustness of mode locking to different values of the Henry factors for the gain medium and the absorber (see Fig. 7(c)). This result is reminiscent of previous works applied to standard semiconductor lasers [55–59], in which the difference between the Henry factors was found to be detrimental to mode locking. In our case, we find that this difference between the Henry factors reduces the robustness of the nanolaser mode locking to potential disorders.

In Ref. [16], we found that the dynamical behaviors of the lasers were similar in the situations where the gain and the absorber overlap or are separated inside the cavity. We thus also investigate here the robustness of the laser mode-locking to potential disorder in the situation where the gain and the absorber do no longer overlap. The values of the parameters as the same as before, except that the gain region is located in the region $-2.5\ x_\Omega \le x \le 0$ and the absorber in the region $0 \le x \le 2.5\ x_\Omega$. The results are plotted as dashed lines in Figs. 7(a),(b), and (d). In Fig. 7(a), for separated gain and absorber regions, $\delta_{C,th}$ is found to increase with r_a for $r_g = 150$. One significant difference with respect to the case where the two media overlap is that $\delta_{C,th}$ is divided by a factor of 2. This is due to the fact that the pulse just stays only half of the time in the absorber region. The effective absorption for the whole field is then only one half of its value, leading to a reduction of $\delta_{C,th}$ to one half of its value when the absorber fills both sides of the resonator. The same results are observed for the investigation of the robustness to the Henry factors with $r_g = 150$ and $r_g = 10$ in Fig. 7(b) and Fig. 7(d).

Optics EXPRESS

4. Conclusion

In this paper, we have theoretically analyzed the robustness of the mode locked regime of oscillation in a harmonic cavity nanolaser, sustaining oscillation of Hermite-Gaussian modes, to imperfections of its harmonic potential. First, we considered the effect of the non-parabolicity of the potential. A fourth-order term was introduced to quantify the distortion of the potential, which leads to shifts of the eigenfrequencies. We found that locking the modes using a saturable absorber can to some extent compensate for this distortion.

Moreover, the more general case of random errors in the potential has been statistically analyzed by calculating the relative root mean square (RMS) deviation δ_C of the comb frequencies. By comparing the distribution of δ_C for the locked solutions with that for all the solutions, we could obtain the evolution of the threshold value $\delta_{C,th}$ with the laser parameters. The robustness of mode locking to disorder was found to increase with the saturable absorption rate on the condition that the gain is large enough to keep the laser away from the Q-switching regime. A well-chosen value for the Henry factors has been shown to increase the robustness of the mode-locked regime. Similar results are obtained for the robustness of the laser to the non-parabolicity of the potential and are reported in Supplement 1.

Acknowledgement. This work was performed in the framework of the joint lab between Thales Research & Technology and LuMIn.

Disclosures. The authors declare no conflicts of interest.

Supplemental document. See Supplement 1 for supporting content.

References

1. S. Kawanishi, "Ultrahigh-speed optical time-division-multiplexed transmission technology based on optical signal processing," IEEE J. Quantum Electron. **34**(11), 2064–2079 (1998).
2. D. Huang, E. A. Swanson, C. P. Lin, J. S. Schuman, W. G. Stinson, W. Chang, M. R. Hee, T. Flotte, K. Gregory, C. A. Puliafito, and J. G. Fujimoto, "Optical coherence tomography," Science **254**(5035), 1178–1181 (1991).
3. P. Ghelfi, F. Laghezza, F. Scotti, G. Serafino, A. Capria, S. Pinna, D. Onori, C. Porzi, M. Scaffardi, A. Malacarne, V. Vercesi, E. Lazzeri, F. Berizzi, and A. Bogoni, "A fully photonics-based coherent radar system," Nature **507**(7492), 341–345 (2014).
4. J. Kim, J. A. Cox, J. Chen, and F. X. Kärtner, "Drift-free femtosecond timing synchronization of remote optical and microwave sources," Nat. Photonics **2**(12), 733–736 (2008).
5. A. Khilo, S. J. Spector, M. E. Grein, A. H. Nejadmalayeri, C. W. Holzwarth, M. Y. Sander, M. S. Dahlem, M. Y. Peng, M. W. Geis, N. A. DiLello, J. U. Yoon, A. Motamedi, J. S. Orcutt, J. P. Wang, C. M. Sorace-Agaskar, M. A. Popović, J. Sun, G.-R. Zhou, H. Byun, J. Chen, J. L. Hoyt, H. I. Smith, R. J. Ram, M. Perrott, T. M. Lyszczarz, E. P. Ippen, and F. X. Kärtner, "Photonic ADC: overcoming the bottleneck of electronic jitter," Opt. Express **20**(4), 4454 (2012).
6. K. C. Phillips, H. H. Gandhi, E. Mazur, and S. K. Sundaram, "Ultrafast laser processing of materials: a review," Adv. Opt. Photonics **7**(4), 684 (2015).
7. S. A. Diddams, L. Hollberg, and V. Mbele, "Molecular fingerprinting with the resolved modes of a femtosecond laser frequency comb," Nature **445**(7128), 627–630 (2007).
8. I. Coddington, W. C. Swann, and N. R. Newbury, "Coherent multiheterodyne spectroscopy using stabilized optical frequency combs," Phys. Rev. Lett. **100**(1), 013902 (2008).
9. D. J. Derickson, R. J. Helkey, A. Mar, J. R. Karin, J. G. Wasserbauer, and J. E. Bowers, "Short Pulse Generation Using Multisegment Mode-Locked Semiconductor Lasers," IEEE J. Quantum Electron. **28**(10), 2186–2202 (1992).
10. E. A. Avrutin, J. H. Marsh, and E. L. Portnoi, "Monolithic and multi-GigaHertz mode-locked semiconductor lasers: Constructions, experiments, models and applications," IEE Proc.: Optoelectron. **147**(4), 251–278 (2000).
11. R. M. Ma and R. F. Oulton, "Applications of nanolasers," Nat. Nanotechnol. **14**(1), 12–22 (2019).
12. S. Combrié, G. Lehoucq, G. Moille, A. Martin, and A. De Rossi, "Comb of high-Q Resonances in a Compact Photonic Cavity," Laser Photonics Rev. **11**(6), 1700099 (2017).
13. G. Marty, S. Combrié, F. Raineri, and A. De Rossi, "Photonic Crystal Optical Parametric Oscillator," Nat. Photonics **15**(1), 53–58 (2021).
14. G. Marty, S. Combrié, A. De Rossi, and F. Raineri, "Hybrid InGaP nanobeam on silicon photonics for efficient four wave mixing," APL Photonics **4**(12), 120801 (2019).
15. Y. Sun, S. Combrié, F. Bretenaker, and A. De Rossi, "Mode Locking of the Hermite-Gaussian Modes of a Nanolaser," Phys. Rev. Lett. **123**(23), 233901 (2019).
16. Y. Sun, S. Combrié, A. De Rossi, and F. Bretenaker, "Dynamics of mode-locked nanolasers based on Hermite-Gaussian modes," Phys. Rev. A **102**(4), 043503 (2020).

Optics EXPRESS

17. T. Prasad, V. L. Colvin, and D. M. Mittleman, "The effect of structural disorder on guided resonances in photonic crystal slabs studied with terahertz time-domain spectroscopy," Opt. Express **15**(25), 16954–16965 (2007).
18. D. Gerace and L. C. Andreani, "Effects of disorder on propagation losses and cavity Q-factors in photonic crystal slabs," Photonics Nanostruct. - Fundamentals Appl. **3**(2-3), 120–128 (2005).
19. S. Fan, P. R. Villeneuve, and J. D. Joannopoulos, "Theoretical investigation of fabrication-related disorder on the properties of photonic crystals," J. Appl. Phys. **78**(3), 1415–1418 (1995).
20. K. C. Kwan, X. Zhang, Z. Q. Zhang, and C. T. Chan, "Effects due to disorder on photonic crystal-based waveguides," Appl. Phys. Lett. **82**(25), 4414–4416 (2003).
21. T. N. Langtry, A. A. Asatryan, L. C. Botten, C. M. de Sterke, R. C. McPhedran, and P. A. Robinson, "Effects of disorder in two-dimensional photonic crystal waveguides," Phys. Rev. E **68**(2), 026611 (2003).
22. A. A. Asatryan, P. A. Robinson, L. C. Botten, R. C. McPhedran, N. A. Nicorovici, and C. Martijn De Sterke, "Effects of geometric and refractive index disorder on wave propagation in two-dimensional photonic crystals," Phys. Rev. E **62**(4), 5711–5720 (2000).
23. L. O'Faolain, T. P. White, D. O'Brien, X. Yuan, M. D. Settle, and T. F. Krauss, "Dependence of extrinsic loss on group velocity in photonic crystal waveguides," Opt. Express **15**(20), 13129–13138 (2007).
24. E. R. Méndez, E. E. García-Guerrero, T. A. Leskova, A. A. Maradudin, J. Muñoz-López, and I. Simonsen, "Design of one-dimensional random surfaces with specified scattering properties," Appl. Phys. Lett. **81**(5), 798–800 (2002).
25. R. Ferrini, D. Leuenberger, R. Houdré, H. Benisty, M. Kamp, and A. Forchel, "Disorder-induced losses in planar photonic crystals," Opt. Lett. **31**(10), 1426–1428 (2006).
26. T. A. Leskova, A. A. Maradudin, I. V. Novikov, A. V. Shchegrov, and E. R. Méndez, "Design of one-dimensional band-limited uniform diffusers of light," Appl. Phys. Lett. **73**(14), 1943–1945 (1998).
27. A. Rodriguez, M. Ibanescu, J. D. Joannopoulos, and S. G. Johnson, "Disorder-immune confinement of light in photonic-crystal cavities," Opt. Lett. **30**(23), 3192–3194 (2005).
28. H. Li, B. Cheng, and D. Zhang, "Two-dimensional disordered photonic crystals with an average periodic lattice," Phys. Rev. B **56**(17), 10734–10736 (1997).
29. H. Li, H. Chen, and X. Qiu, "Band-gap extension of disordered 1D binary photonic crystals," Phys. B **279**(1-3), 164–167 (2000).
30. M. M. Sigalas, C. M. Soukoulis, C. T. Chan, R. Biswas, and K. M. Ho, "Effect of disorder on photonic band gaps," Phys. Rev. B **59**(20), 12767–12770 (1999).
31. Y. A. Vlasov, M. A. Kaliteevski, and V. V. Nikolaev, "Different regimes of light localization in a disordered photonic crystal," Phys. Rev. B **60**(3), 1555–1562 (1999).
32. Z. Y. Li and Z. Q. Zhang, "Fragility of photonic band gaps in inverse-opal photonic crystals," Phys. Rev. B **62**(3), 1516–1519 (2000).
33. E. Lidorikis, M. Sigalas, E. Economou, and C. Soukoulis, "Gap deformation and classical wave localization in disordered two-dimensional photonic-band-gap materials," Phys. Rev. B **61**(20), 13458–13464 (2000).
34. M. Patterson, S. Hughes, S. Combrié, N. V. Tran, A. De Rossi, R. Gabet, and Y. Jaouën, "Disorder-induced coherent scattering in slow-light photonic crystal waveguides," Phys. Rev. Lett. **102**(25), 253903 (2009).
35. L. Braginsky and V. Shklover, "Light propagation in an imperfect photonic crystal," Phys. Rev. B **73**(8), 085107 (2006).
36. M. A. Kaliteevski, J. M. Martinez, D. Cassagne, and J. P. Albert, "Disorder-induced modification of the transmission of light in a two-dimensional photonic crystal," Phys. Rev. B **66**(11), 113101 (2002).
37. W. R. Frei and H. T. Johnson, "Finite-element analysis of disorder effects in photonic crystals," Phys. Rev. B **70**(16), 165116 (2004).
38. J. P. Vasco and V. Savona, "Disorder effects on the coupling strength of coupled photonic crystal slab cavities," New J. Phys. **20**(7), 075002 (2018).
39. G. Fujii, T. Matsumoto, T. Takahashi, and T. Ueta, "Study on transition from photonic-crystal laser to random laser," Opt. Express **20**(7), 7300–7315 (2012).
40. M. Leonetti, C. Conti, and C. Lopez, "The mode-locking transition of random lasers," Nat. Photonics **5**(10), 615–617 (2011).
41. F. Antenucci, C. Conti, A. Crisanti, and L. Leuzzi, "General phase diagram of multimodal ordered and disordered lasers in closed and open cavities," Phys. Rev. Lett. **114**(4), 043901 (2015).
42. Y. Lahini, A. Avidan, F. Pozzi, M. Sorel, R. Morandotti, D. N. Christodoulides, and Y. Silberberg, "Anderson localization and nonlinearity in one-dimensional disordered photonic lattices," Phys. Rev. Lett. **100**(1), 013906 (2008).
43. T. Schwartz, G. Bartal, S. Fishman, and M. Segev, "Transport and Anderson localization in disordered two-dimensional photonic lattices," Nature **446**(7131), 52–55 (2007).
44. A. A. Chabanov, M. Stoytchev, and A. Z. Genack, "Statistical signatures of photon localization," Nature **404**(6780), 850–853 (2000).
45. P. D. García and P. Lodahl, "Physics of Quantum Light Emitters in Disordered Photonic Nanostructures," Ann. Phys. **529**(8), 1600351 (2017).
46. S. Yu, C. W. Qiu, Y. Chong, S. Torquato, and N. Park, "Engineered disorder in photonics," *Nat. Rev. Mater.*, pp. 1–18 (2020).

Optics EXPRESS

47. B. Rigal, D. Drahi, C. Jarlov, B. Dwir, A. Rudra, I. Kulkova, A. Lyasota, and E. Kapon, "Probing disorder and mode localization in photonic crystal cavities using site-controlled quantum dots," J. Appl. Phys. **123**(4), 043109 (2018).
48. M. Balasubrahmaniyam and S. Mujumdar, "Direct experimental determination of critical disorder in one-dimensional weakly disordered photonic crystals," Phys. Rev. B **98**(18), 184203 (2018).
49. K. G. Makris, A. Brandstötter, P. Ambichl, Z. H. Musslimani, and S. Rotter, "Wave propagation through disordered media without backscattering and intensity variations," Light: Sci. Appl. **6**(9), e17035 (2017).
50. A. Brandstötter, K. G. Makris, and S. Rotter, "Scattering-free pulse propagation through invisible non-Hermitian media," Phys. Rev. B **99**(11), 115402 (2019).
51. L. G. Wright, P. Sidorenko, H. Pourbeyram, Z. M. Ziegler, A. Isichenko, B. A. Malomed, C. R. Menyuk, D. N. Christodoulides, and F. W. Wise, "Mechanisms of spatiotemporal mode-locking," Nat. Phys. **16**(5), 565–570 (2020).
52. L. G. Wright, D. N. Christodoulides, and F. W. Wise, "Spatiotemporal mode-locking in multimode fiber lasers," Science **358**(6359), 94–97 (2017).
53. L. G. Wright, Z. Liu, D. A. Nolan, M. J. Li, D. N. Christodoulides, and F. W. Wise, "Self-organized instability in graded-index multimode fibres," Nat. Photonics **10**(12), 771–776 (2016).
54. K. Krupa, A. Tonello, B. M. Shalaby, M. Fabert, A. Barthélémy, G. Millot, S. Wabnitz, and V. Couderc, "Spatial beam self-cleaning in multimode fibres," Nat. Photonics **11**(4), 237–241 (2017).
55. A. G. Vladimirov and D. Turaev, "Model for passive mode locking in semiconductor lasers," Phys. Rev. A **72**(3), 033808 (2005).
56. A. G. Vladimirov, A. S. Pimenov, and D. Rachinskii, "Numerical study of dynamical regimes in a monolithic passively mode-locked semiconductor laser," IEEE J. Quantum Electron. **45**(5), 462–468 (2009).
57. M. Heuck, S. Blaaberg, and J. Mørk, "Theory of passively mode-locked photonic crystal semiconductor lasers," Opt. Express **18**(17), 18003–18014 (2010).
58. C. Schelte, J. Javaloyes, and S. V. Gurevich, "Dynamics of temporally localized states in passively mode-locked semiconductor lasers," Phys. Rev. A **97**(5), 053820 (2018).
59. S. V. Gurevich and J. Javaloyes, "Spatial instabilities of light bullets in passively-mode-locked lasers," Phys. Rev. A **96**(2), 023821 (2017).